Proceedings of CONF-APMM 2025 Symposium: Simulation and Theory of Differential-Integral Equation in Applied Physics
DOI: 10.54254/2753-8818/2025.DL27345

A Novel Collocation Method to Solve the Periodic Orbits: Application to the Circular Restricted Three-Body Problem

Patrick Li

BASIS Independent Silicon Valley, San Jose, USA
patrick.li12138@gmail.com

Abstract. We develop a novel collocation method to solve for stable closed orbits in a static/periodic potential field. Periodic orbits in the Circular Restricted Three-Body Problem (CR3BP) form the foundation of dynamics in binary-star systems, but are usually computed via costly shooting methods or long N -body integrations; a fast, direct solver for closed orbits can therefore help find stability regions and provide high-quality initial conditions for follow-up simulations. We apply it to the CR3BP, finding closed trajectories that may resemble planet orbits in a binary star system or pressure-less streamlines in tidally distorted accretion disks, consistent with orbits found by more traditional methods. In tests with $\frac{M_1}{M_1+M_2} = 0.8$ and n = 64–128 collocation points, the solver converges in 5–13 Newton steps to residual norms $\lesssim 10^{-13}$ with wall-clock times of 0.2–0.8 s per orbit. For the same setup, closed circumbinary (P-type) orbits require $\omega < -0.3$, implying ap/abin $\gtrsim (1+\omega)^{-2/3} \approx 1.3$. Around the primary, closed circumstellar (S-type) orbits require $\omega > 1.8$, implying $a_p/a_{bin} \lesssim (1 + \omega)^{-2/3} M_1^{1/3} \approx 0.47$.

Keywords: methods: numerical, celestial mechanics, three-body problem, periodic orbits, circumbinary planets (P-type), circumstellar planets (S-type), binaries: general, planets and satellites: dynamical evolution and stability, accretion, accretion disks, spectral collocation

1. Introduction

1.1. Exoplanets

Over the past thirty years, the study of exoplanetary systems has transformed our understanding of planet formation and the diversity of planetary systems. Since the discovery of 51 Pegasi b in 1995 [1], astronomers have confirmed nearly ten thousand exoplanets using a variety of detection techniques—including radial velocity, transit photometry, direct imaging, microlensing, and astrometry—which together show a wide range of planetary masses (from sub-Earth to super-Jupiter), orbital architectures, and bulk compositions [2-3].

Nevertheless, two fundamental questions continue to challenge the field. First, the search for habitable worlds remains incomplete: although thousands of small, potentially rocky exoplanets have been found, few lie within the conservative habitable zone of Sun-like stars [4]. Second, the

© 2026 The Authors. This is an open access article distributed under the terms of the Creative Commons Attribution License 4.0 (https://creativecommons.org/licenses/by/4.0/).

DOI: 10.54254/2753-8818/2025.DL27345

physical processes governing the formation and long-term dynamical evolution of planets—particularly in complex gravitational environments—are not yet fully understood [5].

1.2. Circumbinary planets

One intriguing subset of exoplanetary systems is circumbinary planets (CBPs), which orbit around two stars rather than one. CBPs are difficult to observe and confirm. They are typically discovered via high-precision transit surveys (e.g., Kepler and TESS), which can detect the characteristic transit signatures as the planet crosses each star [6-7]. The handful of systems identified so far—such as Kepler-16b, Kepler-47b–d, and TOI-1338b—exhibit a diversity of orbital separations (a few tenths to several astronomical units) and host-binary configurations (eccentricities up to $\sim$0.5), suggesting a variety of formation pathways and migration histories [8-9].

To date, only 32 CBPs have been confirmed [10]—out of nearly ten thousand known exoplanets—implying an occurrence rate of order 10^{-3} [11-12]. This low yield raises the question of whether CBP systems can achieve long-term dynamical stability, and if so, what specific orbital parameters permit their survival. Theoretically, CBPs present a challenging three-body problem: unlike planets around single stars, their orbits must navigate the time-varying gravitational potential of the binary, which can lead to chaotic evolution and ejection on Myr timescales [13]. Yet observations show that more than 30% of Sun-like stars reside in binary or higher-order multiple systems [14], underscoring the importance of understanding how planet formation and stability proceed in such environments. Moreover, close binaries can host rich astrophysical phenomena—ranging from mass transfer to X-ray emission in compact-object binaries—that may influence planet survival and evolution [15].

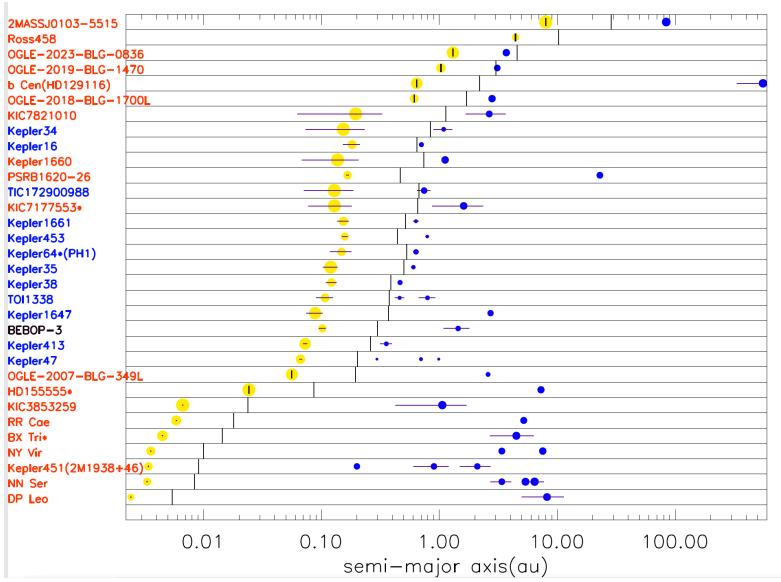

Figure 1. Semi-major axis ap versus host-binary separation abin for confirmed circumbinary planets (CBPs) compiled by The Extrasolar Planets Encyclopaedia [10]. In this plot, the yellow and blue filled circles represent the secondary star and the planet. Most known CBPs reside just outside empirically inferred stability boundaries. (Data accessed August 2025; source: https://exoplanet.eu/planets_binary_circum/.)

Fig. 1 summarizes all the CBPs discovered so far [10]. As shown in the plot, we provide name, the semi-major axes of the secondary star (the yellow filled circles) a_{bin} and the planet (the blue

DOI: 10.54254/2753-8818/2025.DL27345

filled circles) a_p. Clearly, most of the sources have $a_{bin} \sim 0.1 - 1$ au, with several ones that have $a_{bin} < 0.01$ au. Interestingly, the planet a_p in the system whose abin are small has a relatively large a_p/a_{bin}.

To complement Fig. 1, Fig. 2 shows the distribution of host–binary semi-major axes for systems with confirmed S-type planets compiled from The Extrasolar Planets Encyclopaedia [10]. The cyan histogram gives the observed a_{bin} distribution; the solid curve overlays the normalized canonical binary-separation distribution for nearby field stars [14]. The two distributions differ markedly, consistent with a real depletion of planet-hosting tight binaries [16-18] together with known observational biases.

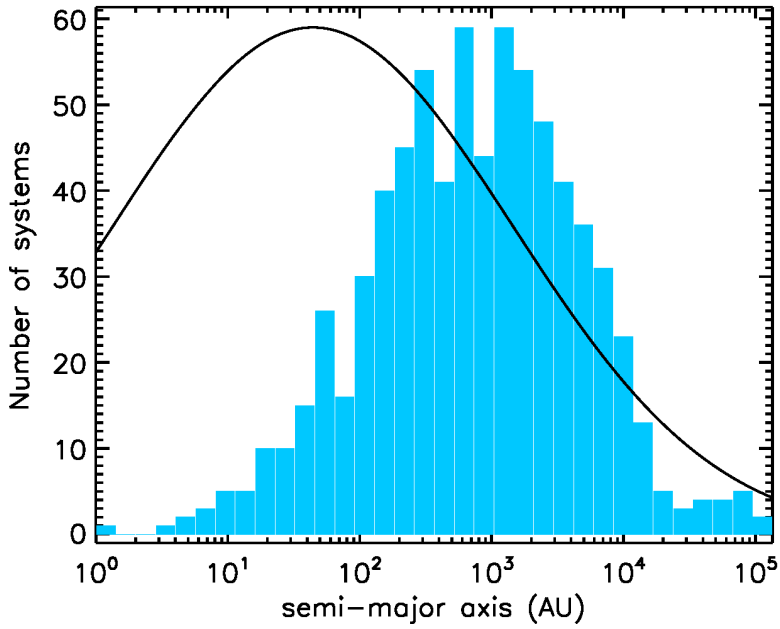

Figure 2. Histogram of host–binary semi-major axes abin for systems hosting S-type planets [10]. Bars show counts per logarithmic bin; the solid curve is the normalized canonical binary-separation distribution for nearby field stars [14]. (Data accessed August 2025; source: https://exoplanet.eu/planets_binary/.)

Previous theoretical investigations of CBP stability have relied primarily on large calculations of N -body integrations, identifying empirical “stability limits” as a function of binary mass ratio, eccentricity, and planet semimajor axis [19-20]. While these studies have mapped out the broad regions of parameter space where CBPs can persist, they are computationally intensive and offer limited insight into the underlying dynamical structure.

1.3. Periodic motions around binary masses

Periodic orbits of planets in and around close binary systems have been extensively investigated. Ref. [21] identified a family of stable CR3BP orbits that can represent both stable gas streamlines in a circumstellar disk (CSD) when gas pressure and viscosity are low and S-type planet orbits near a primary star within a binary system. S-type orbits are near-circular close to one of the binary components, while becoming distorted when the orbital radius becomes large. Constraints were derived for the size of the CSD in binaries with various primary mass ratios. Later, Ref. [22] focused on the properties of P-type, or circumbinary, orbits that encircle both the primary and the secondary. Circumbinary orbits tend to circularize far from the binary, but become tidally distorted at smaller

DOI: 10.54254/2753-8818/2025.DL27345

radii; inner size limits arise that restrict where gas and planets can exist, consistent with subsequent N -body work [19,22].

1.4. Solutions of the Circular Restricted Three-body Problem (CR3BP)

Typically, orbits around close binary systems do not admit analytic solutions, and recent approaches involve simulations that are usually computed via a resource-intensive iterative shooting method and direct integration of the equations of motion. For example, Ref. [19] employed a grid interpolation method based on ∼150 million N -body simulations to determine stability limits of circumbinary planets with various initial parameters. Furthermore, Ref. [23] developed an automated algorithm to search for small circumbinary planets, relying on N -body integrations and significant computational resources.

1.5. Our work

Here, we introduce a new approach that efficiently computes closed S-type and P-type orbits. The technique exploits orbital periodicity, approximating trajectories and their derivatives through linear transformations of Fourier basis functions and spectral differentiation matrices, and thus does not rely on integrals of motion. By assuming periodicity, the differential equations of motion are transformed into algebraic equations that are significantly cheaper to solve, where classic numerical methods like Newton's method are effective. This method rapidly produces accurate orbits consistent with previous studies [21-22], the stability limits of CBP systems [19], and gas-disc morphologies in circumstellar and circumbinary systems [24], while using modest computational resources. The framework can be generalized to periodic orbits in other stationary or rotating potentials.

For a representative mass ratio $\mu = 0.2$ ($M_1 = 0.8$), our solver with n = 64–128 collocation points converges in 5–13 Newton steps to residual norms $\lesssim 10^{-13}$ with wall-clock times of 0.2–0.8 s per orbit. In the same setup we find that closed circumbinary (P-type) solutions exist only for $\omega < -0.3$, which—under the Keplerian mapping used here—corresponds to $a_p/a_{bin} \gtrsim (1 + \omega)^{-2/3} \approx 1.3$. Around the primary, closed circumstellar (S-type) solutions require $\omega > 1.8$, implying $a_p/a_{bin} \lesssim (1 + \omega)^{-2/3} M_1^{1/3} \approx 0.47$. These thresholds provide a compact way to summarize where our periodic-orbit families exist in frequency (and radius) space and are qualitatively consistent with the observed preference against planet-hosting tight binaries and with the distribution of S-type binary separations (see Fig. 1 and the S-type histogram).

This paper is organized as follows. Section 2 develops the periodic-orbit collocation scheme in a rotating frame: we define the gravitational potential Φ, introduce the equispaced Fourier collocation grid and the spectral differentiation matrices D and D_2, and assemble the nonlinear residual system together with the Newton–Raphson Jacobian used to solve it. Section 3 specializes the method to the circular restricted three-body problem (CR3BP) in dimensionless units, defines the gravitational potential U and its derivatives, and applies the solver to three families of solutions: (i) P-type (circumbinary) orbits, (ii) S-type (circumstellar) orbits, and (iii) eccentric-binary snapshots. The Appendix summarizes implementation details of the accompanying Python package, including input parameters, algorithmic pseudocode, and outputs.

DOI: 10.54254/2753-8818/2025.DL27345

2. A collocation method for solving periodic orbits in a static potential field

In this work, we limit ourselves that: 1), all the three celestial bodies are coplanar. 2) the planet is much less massive than the two stars, i.e. the gravity of the planet only serves as a perturber to the binary system.

With the above simplification, consider a test particle in a rotating frame with angular velocity Ω (Ω here is specified to the orbital angular velocity of two stars), under a time-independent potential Φ(x, y) that is static in the corotating frame, i.e.

$$\Phi = -\frac{GM_1}{\sqrt{(x-x_1)^2+y^2}} - \frac{GM_2}{\sqrt{(x-x_2)^2+y^2}} \tag{1}$$

where $x_1 = -\frac{M_2}{M} a_{bin}$, $x_2 = -\frac{M_1}{M} a_{bin}$. If the binary is on circular orbit, the potential is static in a corotating frame. $-\nabla\Phi$ therefore excludes non-inertial Coriolis and centrifugal terms, which appear explicitly below.Let r(t) = (x(t), y(t)) be periodic with phase θ = ωt = 2πt/T , where T is the period in the corotating frame.

The time-domain equations of motion are

$$\begin{aligned} \frac{\partial^2 x}{\partial t^2} - 2\Omega\frac{\partial y}{\partial t} - \Omega^2 x + \frac{\partial \Phi}{\partial x} &= 0, \\ \frac{\partial^2 y}{\partial t^2} + 2\Omega\frac{\partial x}{\partial t} - \Omega^2 y + \frac{\partial \Phi}{\partial y} &= 0. \end{aligned} \tag{2}$$

Introducing the phase variable θ with T = 2π/ω gives

$$\begin{aligned} \omega^2\frac{\partial^2 x}{\partial \theta^2} - 2\Omega\omega\frac{\partial y}{\partial \theta} - \Omega^2 x + \frac{\partial \Phi}{\partial x} &= 0, \\ \omega^2\frac{\partial^2 y}{\partial \theta^2} + 2\Omega\omega\frac{\partial x}{\partial \theta} - \Omega^2 y + \frac{\partial \Phi}{\partial y} &= 0. \end{aligned} \tag{3}$$

We apply a (trigonometric) pseudo-spectral collocation method on an equispaced periodic grid,

$$\theta_j = \frac{2\pi j}{n}, j = 0,1,\ldots,n-1, \tag{4}$$

and discretize the solution as xj := x(θj), yj := y(θj). For smooth 2π-periodic functions, the first and second derivatives at the grid points can be represented using the Fourier spectral differentiation matrices [25]:

$$\begin{aligned} \frac{\partial x_j}{\partial \theta} &= \sum_k D_{jk} x_k , \frac{\partial^2 x_j}{\partial \theta^2} = \sum_k (D_2)_{jk} x_k , \\ \frac{\partial y_j}{\partial \theta} &= \sum_k D_{jk} y_k , \frac{\partial^2 y_j}{\partial \theta^2} = \sum_k (D_2)_{jk} y_k . \end{aligned} \tag{5}$$

For the equispaced grid,

$$D_{jk} = \begin{cases} 0, & j = k, \\ \frac{1}{2}(-1)^{j-k}\cot\left[\frac{\pi(j-k)}{n}\right], & j \neq k, \end{cases} \tag{6}$$

DOI: 10.54254/2753-8818/2025.DL27345

$$(D_2)_{jk} = \begin{cases} -\frac{n^2+2}{12}, & j = k, \\ \frac{1}{2}(-1)^{j-k+1}\csc^2\left[\frac{\pi(j-k)}{n}\right], & j \neq k. \end{cases} \tag{7}$$

Evaluating the phase-form equations at θ_j yields the nonlinear algebraic residuals

$$\begin{aligned} \omega^2 \sum_k (D_2)_{jk} x_k - 2\Omega\omega \sum_k D_{jk} y_k - \Omega^2 x_j + \frac{\partial \Phi}{\partial x}\Big|_{x=x_j, y=y_j} = 0, \\ \omega^2 \sum_k (D_2)_{jk} y_k + 2\Omega\omega \sum_k D_{jk} x_k - \Omega^2 y_j + \frac{\partial \Phi}{\partial y}\Big|_{x=x_j, y=y_j} = 0. \end{aligned} \tag{8}$$

which we solve by Newton–Raphson with circular initial guesses. After obtaining $\{x_j\}$, $\{y_j\}$, we reconstruct continuous orbits $x_{int}(\theta)$, $y_{int}(\theta)$ from a truncated Fourier series; a modest number of modes suffices for smooth closed orbits.

Newton–Raphson and Jacobian. To apply Newton–Raphson, we linearize around the current iterate:

$$\mathbf{f}(\mathbf{z}_{n+1}) - \mathbf{f}(\mathbf{z}_n) \approx \nabla \mathbf{f}|_{\mathbf{z}_n} \cdot (\mathbf{z}_{n+1} - \mathbf{z}_n) \equiv \mathbb{J}(\mathbf{z}_n)(\mathbf{z}_{n+1} - \mathbf{z}_n)(\mathbf{z}_{n+1} - \mathbf{z}_n), \tag{9}$$

where the Jacobian is

$$\mathbb{J} = \frac{\partial \mathbf{f}}{\partial \mathbf{z}} = \begin{bmatrix} \frac{\partial f_1}{\partial z_1} & \cdots & \frac{\partial y}{\partial z_m} \\ \vdots & \ddots & \vdots \\ \frac{\partial f_m}{\partial z_1} & \cdots & \frac{\partial f_m}{\partial z_m} \end{bmatrix}. \tag{10}$$

In our problem, each collocation point (x_j , y_j) contributes a local 2 × 2 block from the potential terms, whose entries are listed in Section 3. These blocks are assembled (along the diagonal) together with the spectral differentiation contributions (from D and D_2 in Eq. (8)) to form the global Jacobian used in each Newton update.

3. Application to CR3BP orbits

For this application, we adopt a scale-free normalization of G = Ω = abin = M_1 + M_2 = 1. We also define μ ≡ M_2/(M_1 + M_2), i.e. M_1 = 1 − μ and M_2 = μ. In the corotating (of the binary stars) frame, the stars lie on the x-axis at x_1 = −μ and x_2 = 1 − μ, and the planet–star distances are

$$r_1 = \sqrt{(x+\mu)^2 + y^2},\ r_2 = \sqrt{(x-1+\mu)^2 + y^2}. \tag{11}$$

We now define and work with the (negative) gravitational potential U where

$$U\Big(x, y\Big) = U_1 + U_2 = -\frac{1-\mu}{r_1} - \frac{\mu}{r_2}, \tag{12}$$

whose gradients are

DOI: 10.54254/2753-8818/2025.DL27345

$$\frac{\partial U_1}{\partial x} = \left(1-\mu\right)\frac{x+\mu}{r_1^3},\ \frac{\partial U_1}{\partial y} = \left(1-\mu\right)\frac{y}{r_1^3},\ \frac{\partial U_2}{\partial x} = \mu\frac{x-1+\mu}{r_2^3},\ \frac{\partial U_2}{\partial y} = \mu\frac{y}{r_2^3}. \tag{13}$$

Including the inertial terms of the rotating frame (Coriolis and centrifugal) and using the normalization above, the planar equations of motion become

$$\ddot{x} = -\left(1-\mu\right)\frac{x+\mu}{r_1^3} - \mu\frac{x-1+\mu}{r_2^3} + 2\dot{y} + x, \tag{14}$$

$$\ddot{y} = -\left(1-\right)\mu\frac{y}{r_1^3} - \mu\frac{y}{r_2^3} + 2\dot{x} + y. \tag{15}$$

which provide the force evaluations used in the collocation residuals of Eq. (8).

For Newton updates we use the following second derivatives of U for the entries of Jacobian:

$$U_{xx} = \left(1-\mu\right)\left(\frac{1}{r_1^3} - \frac{3(x+\mu)^2}{r_1^5}\right) + \mu\left(\frac{1}{r_2^3} - \frac{3(x-1+\mu)^2}{r_2^5}\right), \tag{16}$$

$$U_{yy} = \left(1-\mu\right)\left(\frac{1}{r_1^3} - \frac{3y^2}{r_1^5}\right) + \mu\left(\frac{1}{r_2^3} - \frac{3y^2}{r_2^5}\right), \tag{17}$$

$$U_{xy} = -3\left(1-\mu\right)\frac{(x+\mu)y}{r_1^5} - 3\mu\frac{(x-1+\mu)y}{r_2^5}, \tag{18}$$

with $U_{xy} = U_{yx}$.

The Newton–Raphson Jacobian $J = \partial F/\partial z$ has the block form

$$J = \begin{bmatrix} \omega^2 D_2 - I + \mathrm{Diag}\left(U_{xx}\right) & -2\omega D + \mathrm{Diag}\left(U_{xy}\right) \\ +2\omega D + \mathrm{Diag}\left(U_{xy}\right) & \omega^2 D_2 - I + \mathrm{Diag}\left(U_{yy}\right) \end{bmatrix}, \tag{19}$$

where $\mathrm{Diag}(U_{xx})$ denotes the $N \times N$ diagonal matrix whose (j, j) entry is $U_{xx}(x_j, y_j)$, etc.

3.1. Case 1: circumbinary P-type orbits

For $\mu = 0.2$ we find closed circumbinary (P-type) solutions only for $\omega < -0.3$; for $-0.3 \le \omega < 0$ the Newton iterations either fail to converge or lead to self-intersecting trajectories. In our normalization ($G = \Omega = a_{bin} = M_1 + M_2 = 1$), the inertial mean motion is $n = 1 + \omega$. Approximating wide circumbinary motion as Keplerian around the total mass, $n^2\, a_p^3 \simeq 1$, which gives the convenient conversion

$$\frac{a_p}{a_{bin}} \simeq (1+\omega)^{-2/3}. \tag{20}$$

At the measured threshold $\omega = -0.3$, this implies $a_p/a_{bin} \gtrsim (0.7)^{-2/3} \approx 1.3$.

DOI: 10.54254/2753-8818/2025.DL27345

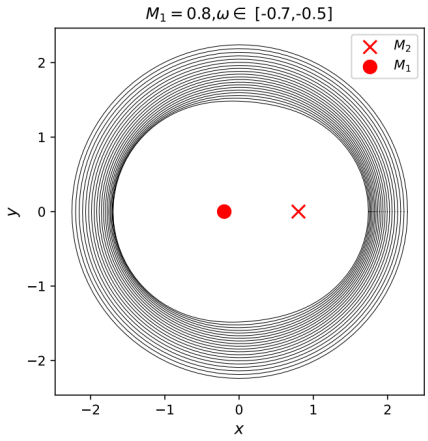

Figure 3. P-type (circumbinary) orbits of the planet for $M_1 = 0.8$, $M_2 = 0.2$. The angular frequency ω ranges from values near −1 (very wide orbits) toward 0^- (approaching corotation), with increasing tidal distortion at larger $n = 1 + \omega$

In our work, we take different values of ω, and then determine if we can find suitable orbits for this chosen ω. For sufficiently negative ω (hence small $n = 1 + \omega$ and large a_p), we robustly find stable solutions that are nearly circular. The mapping above shows that smaller (more negative) ω corresponds to larger a_p/a_{bin}.We consider a system with $\mu = M_2/(M_1 + M_2) = 0.2$ (i.e., $M_1 = 0.8$). Interestingly, we cannot find stable solutions for the positive (corotating) ω branch.

As $\omega \to -1$, the orbit size approaches infinity (the inertial mean motion $n = 1 + \omega \to 0$). As ω increases from −1 toward 0^-, very wide orbits (black lines) remain nearly circular but become tidally distorted closer to the binary; in the opposite limit $\omega \to 0^-$, the paths collapse toward corotating points and self-intersections occur before ω reaches zero. We compared periodic orbits for a broad range of μ with Ref. [22], obtained by direct integration, and find strong qualitative agreement.

3.2. Case 2: circumstellar S-type orbits

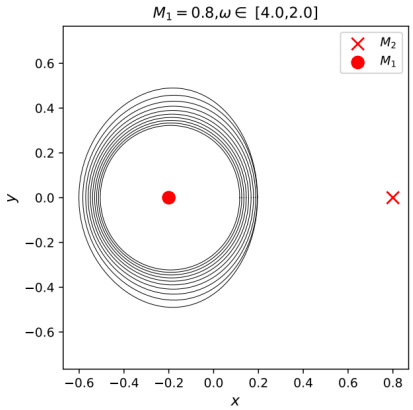

Figure 4. S-type orbits for $M_1 = 0.8$, $M_2 = 0.2$. The orbits are bound to the primary M_1 and become increasingly non-circular as the orbital frequency decreases from large positive ω

Figure 4 shows a set of S-type orbits for $\mu = 0.2$ (orbits around the more massive star M_1). Inner orbits are nearly circular; for sufficiently small $\omega > 0$, orbits become so distorted that intersections

DOI: 10.54254/2753-8818/2025.DL27345

occur.

For the same mass ratio ($\mu = 0.2$, i.e. $M_1 = 0.8$), we find closed circumstellar (S-type) solutions only for $\omega > 1.8$. With $n = 1 + \omega$ and a Keplerian mapping about the primary, $n^2 a_p^3 \simeq M_1$, yielding

$$\frac{a_p}{a_{bin}} \simeq M_1^{1/3}(1+\omega)^{-2/3}. \tag{21}$$

At $\omega = 1.8$ this implies $a_p/a_{bin} \lesssim 0.8^{1/3}\,(2.8)^{-2/3} \approx 0.47$. More complicated morphologies at extreme mass ratios [21] are reproducible with our method.

3.3. Case 3: eccentric orbits

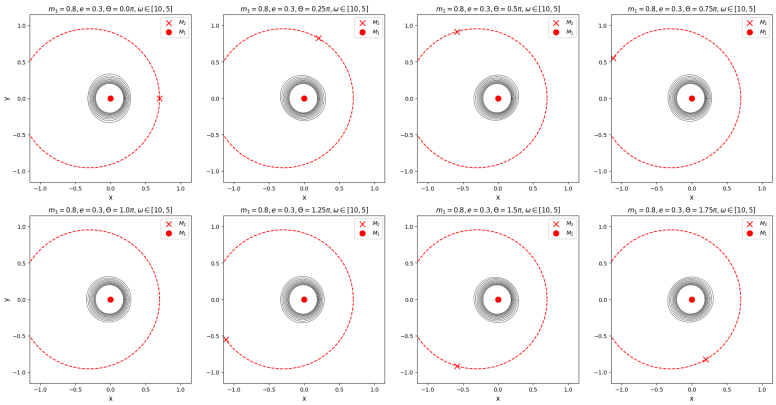

Figure 5. Eccentric S-type orbits for $e = 0.3$ with $M_1 = 0.8$, $M_2 = 0.2$. The binary components are no longer stationary in the corotating frame; we show snapshots at phases $\Theta_i = \Theta_{i-1} + 2\pi/n$ with $n = 8$

When eccentricity is nonzero, corotating frames are not stationary with respect to the binary masses. We therefore switch to the inertial frame and divide the motion into phases, with the secondary moving on an ellipse around the primary following Kepler's law. Kepler's equation relates the mean anomaly M to the eccentric anomaly E as $E - e \sin E = M$. In our implementation, a set of evenly spaced mean anomalies yields the corresponding eccentric anomalies via Newton iterations; the companion's coordinates follow the standard parameterization,

$$x_b = \cos E - e, y_b = \sin E\sqrt{1-e^2}, \tag{22}$$

and the two stellar positions are placed at the barycentric locations $r_1 = -\mu\, r_{rel}$ and $r_2 = (1-\mu)\, r_{rel}$, where $r_{rel} = (x_b, y_b)$. Figure 5 shows representative snapshots comparable to the circular-binary case.

3.4. Convergence and computational cost

In practice we find rapid convergence from circular initial guesses, with 5–15 Newton iterations typical for $n \lesssim 128$.

To document performance, we report in Table 1 the residual norm, which is independent from grid size,as $\|\mathbf{F}\|_2 \frac{\left(\sum_j \left(F_{xj}^2 + F_{yj}^2\right)\right)^{1/2}}{n}$, versus number of iterations, and wall-clock times.

DOI: 10.54254/2753-8818/2025.DL27345

Table 1. Convergence and cost

Case	n	Newton iters	$\log_{10}\|\mathbf{F}\|_2$ (final)	Time [s]
S-type, μ = 0.2, ω = +6	64	5	-12.6	0.2
S-type, μ = 0.2, ω = +3	128	5	-12.8	0.3
P-type, μ = 0.2, ω = −0.6	64	5	-13.6	0.2
P-type, μ = 0.2, ω = −0.3	128	13	-13.7	0.8

4. Conclusion

We presented a Fourier–collocation scheme that solves directly for closed, planar periodic orbits in the CR3BP. By enforcing periodicity at an equispaced grid and using spectral differentiation, the equations of motion reduce to a nonlinear algebraic system that is efficiently solved by Newton updates with an analytically assembled Jacobian. For a representative mass ratio μ = 0.2 (M_1 = 0.8) and n = 64–128 collocation points, the solver converges in 5–13 iterations to residual norms $\lesssim 10^{-13}$ with wall-clock times of 0.2–0.8 s per orbit (Table 1).

Key findings.

• P-type (circumbinary) families: For μ = 0.2 we obtain closed circumbinary solutions only for ω < −0.3; for −0.3 ≤ ω < 0 Newton iterations either fail to converge or yield self-intersections. Using the inertial mean motion n = 1 + ω and a Keplerian mapping about the total mass ($n^2 a_p^3 \simeq 1$ in our normalization), this threshold corresponds to

$$\frac{a_p}{a_{bin}} \simeq (1+\omega)^{-2/3} \Rightarrow \frac{a_p}{a_{bin}} \gtrsim (0.7)^{-2/3} \approx 1.3 \qquad \text{at } \omega = -0.3.$$

• S-type (circumstellar) families: Around the primary (M_1 = 0.8) we find closed circumstellar solutions only for ω > 1.8. With n = 1 + ω and a Keplerian mapping about M_1 ($n2\, a_p^3 \simeq M_1$), we obtain

ap

$$\frac{a_p}{a_{bin}} \simeq M_1^{1/3}(1+\omega)^{-2/3} \Rightarrow \frac{a_p}{a_{bin}} \lesssim 0.8^{1/3}(2.8)^{-2/3} \approx 0.47 \qquad \text{at } \omega = 1.8.$$

These frequency thresholds summarize where our periodic-orbit families exist in (ω, a_p/a_{bin}) space for the tested μ. The broad morphological trends agree with classical families obtained by direct integration [21-22]: wide P-type orbits are nearly circular and become tidally distorted as they approach the binary; S-type orbits are circular near the primary and develop strong distortions before self-intersection.

Context with observations. The P-type requirement of relatively large ap/abin aligns qualitatively with the observed scarcity of close-in circumbinary planets in current catalogs (Fig. 1). For S-type systems, the existence of closed circumstellar families only at relatively small a_p/a_{bin} is consistent with the notion that tighter binaries are disfavored hosts for S-type planets and with the observed distribution of S-type binary separations (Fig. 2). We emphasize that our a_p/a_{bin} translations use simple Keplerian scalings (appropriate for wide orbits) and are intended as order-of-magnitude guides.

Limitations and scope. Our calculations assume planar motion, a circular binary for the main families, and a test particle (no feedback on the binary, no pressure/self-gravity). The eccentric-

DOI: 10.54254/2753-8818/2025.DL27345

binary examples are shown as inertial-frame snapshots rather than true periodic solutions in a single rotating frame. Near strong resonances or where self-intersections develop, the Newton solver may require continuation strategies and/or additional regularization.

Applications and outlook. Because each orbit is obtained with modest cost, the method can (i) provide fast initial guesses for high-accuracy N -body integrations, (ii) map families of closed streamlines relevant to low-pressure gas discs, and (iii) supply priors for stability screening in circumbinary and circumstellar planet searches. Extensions that are worthy of pursuing include pseudo-arclength continuation in ω and μ, fully periodic treatments of eccentric binaries (time-periodic forcing), three-dimensional generalizations, and coupling to weak non-gravitational forces (e.g. pressure or drag) to study disc truncation and gap morphologies.

References

[1] M. Mayor and D. Queloz. A Jupiter-mass companion to a solar-type star. , 378: 355–359, November 1995. doi: 10.1038/378355a0.

[2] J. N. Winn and D. C. Fabrycky. The Occurrence and Architecture of Exoplanetary Systems. , 53: 409–447, 2015. doi: 10.1146/annurev-astro-082214-122246.

[3] R. I. Dawson and J. A. Johnson. Origins of Hot Jupiters. , 56: 175–221, 2018. doi: 10.1146/ annurev-astro-081817-051853.

[4] R. K. Kopparapu, R. Ramirez, J. F. Kasting, V. Eymet, T. D. Robinson, S. Mahadevan, R. C. Terrien, S. Domagal-Goldman, V. Meadows, and R. Deshpande. Habitable Zones Around Main-Sequence Stars: New Estimates. , 765(2): 131, March 2013. doi: 10.1088/0004-637X/765/2/131.

[5] A. Morbidelli and S. N. Raymond. Challenges in planet formation. Journal of Geophysical Research: Planets, 121(10): 1962–1980, 2016. doi: 10.1002/2016JE005088.

[6] L. R. Doyle, J. A. Carter, D. C. Fabrycky, R. W. Slawson, S. B. Howell, J. N. Winn, J. A. Orosz, and others. Kepler-16: A Transiting Circumbinary Planet. Science, 333(6049): 1602–1606, September 2011. doi: 10.1126/science.1210923.

[7] V. B. Kostov, J. A. Orosz, W. F. Welsh, B. Cale, B. Quarles, N. Haghighipour, and others. TOI-1338 b: TESS's First Transiting Circumbinary Planet. , 159: 253, 2020. doi: 10.3847/1538-3881/ab5d3a.

[8] W. F. Welsh, J. A. Orosz, J. A. Carter, D. C. Fabrycky, and others. Transiting circumbinary planets Kepler-34 and Kepler-35. , 481: 475–479, January 2012. doi: 10.1038/nature10768.

[9] J. A. Orosz, W. F. Welsh, N. Haghighipour, B. Quarles, D. R. Short, S. M. Mills, S. Satyal, and others.Discovery of a Third Transiting Planet in the Kepler-47 Circumbinary System. , 157(5): 174, May 2019. doi: 10.3847/1538-3881/ab0ca0.

[10] J. Schneider, C. Dedieu, P. Le Sidaner, R. Savalle, and I. Zolotukhin. Defining and cataloging exoplanets: the exoplanet.eu database. Astronomy & Astrophysics, 532: A79, 2011. doi: 10.1051/0004-6361/201116713. URL https: //exoplanet.eu/.

[11] D. J. Armstrong, H. P. Osborn, D. J. A. Brown, F. Faedi, Y. G´omez Maqueo Chew, D. V. Martin, D. Pollacco, and S. Udry. On the abundance of circumbinary planets. , 444(2): 1873–1883, November 2014. doi: 10.1093/mnras/stu1590.

[12] D. V. Martin and A. H. M. J. Triaud. Circumbinary planets – why they are so likely to transit. , 449(1): 781–792, May 2015. doi: 10.1093/mnras/stv228.

[13] M. J. Holman and P. A. Wiegert. Long-Term Stability of Planets in Binary Systems. , 117(1): 621–628, January 1999. doi: 10.1086/300695.

[14] D. Raghavan, H. A. McAlister, T. J. Henry, D. W. Latham, G. W. Marcy, B. D. Mason, D. R. Gies, R. J. White, and T. A. ten Brummelaar. A Survey of Stellar Families: Multiplicity of Solar-type Stars. , 190 (1): 1–42, January 2010. doi: 10.1088/0067-0049/190/1/1.

[15] J. Burkart, E. Quataert, P. Arras, and N. N. Weinberg. Tidal asteroseismology: distortion and mass loss in eccentric binary stars. , 421(2): 983–993, April 2012. doi: 10.1111/j.1365-2966.2011.20365.x.

[16] Adam L. Kraus, Michael J. Ireland, Daniel Huber, Andrew W. Mann, and Trent J. Dupuy. The Impact of Stellar Multiplicity on Planetary Systems. I. The Ruinous Influence of Close Binary Companions. , 152 (1): 8, July 2016. doi: 10.3847/0004-6256/152/1/8.

[17] Lea A. Hirsch, David R. Ciardi, Andrew W. Howard, Mark E. Everett, Elise Furlan, Mindy Saylors, Elliott P. Horch, Steve B. Howell, Johanna Teske, and Geoffrey W. Marcy. Assessing the Effect of Stellar Companions from

DOI: 10.54254/2753-8818/2025.DL27345

High-resolution Imaging of Kepler Objects of Interest. , 153(3): 117, March 2017. doi: 10.3847/ 1538-3881/153/3/117.
[18] Carl Ziegler, Andrei Tokovinin, Madelyn Latiolais, C´esar Brice˜no, Nicholas Law, and Andrew W. Mann. SOAR TESS Survey. II. The Impact of Stellar Companions on Planetary Populations. , 162(5): 192, November 2021. doi: 10.3847/1538-3881/ac17f6.
[19] B. Quarles, S. Satyal, V. Kostov, N. Kaib, and N. Haghighipour. Stability Limits of Circumbinary Planets: Is There a Pile-up in the Kepler CBPs? , 856(2): 150, April 2018. doi: 10.3847/1538-4357/aab264.
[20] B. Quarles, G. Li, V. B. Kostov, and N. Haghighipour. Orbital Stability of Circumstellar Planets in Binary Systems. , 159: 80, March 2020. doi: 10.3847/1538-3881/ab64fa.
[21] B. Paczynski. A model of accretion disks in close binaries. , 216: 822–826, September 1977. doi: 10.1086/ 155526.
[22] B. Rudak and B. Paczynski. Outer excretion disk around a close binary. , 31(1): 13–24, January 1981.
[23] David V. Martin and Daniel C. Fabrycky. Searching for small circumbinary planets. i. the stanley automated algorithm and no new planets in existing systems. The Astronomical Journal, 162(3): 84, aug 2021. doi: 10.3847/1538-3881/abeab1. URL https: //dx.doi.org/10.3847/1538-3881/abeab1.
[24] Barbara Pichardo, Linda S. Sparke, and Luis A. Aguilar. Circumstellar and circumbinary discs in eccentric stellar binaries. , 359(2): 521–530, May 2005. doi: 10.1111/j.1365-2966.2005.08905.x.
[25] John P Boyd. Chebyshev and Fourier spectral methods. Courier Corporation, 2001.

Appendix

The input parameters of our model are listed in input.txt, which will be read by our Python code:

• m1: Mass of the primary in units of total mass. (Note that our model assumes the total mass of the binary stars is unity.)

• omegamin, omegamax: Minimum and maximum angular frequency ω in units of Ω (the angular velocity of the binary stars).

• omegaN: Number of linearly sampled points in frequency space.

• h, tol, maxit: Learning rate (h), tolerance (tol), and maximum iterations (maxit) for Newton–Raphson.

• N: Number of collocation points over an orbital period.

• type: Orbit type (S for S-type with $\omega > 0$; P for P-type with $-\Omega < \omega < 0$).

The algorithm of our code can be simplified as below.

Algorithm 1. Main function for orbit solver

	Require: X, Y, tol, maxit, h, omegamin, omegamax, omegaN
1:	Generate a list of ω values linearly spaced between omegamin and omegamax with omegaN points
2:	for each ω in the list do
3:	Initialize residuals: F_x, F_y
4:	Compute initial error: errorfunc ← $\sqrt{\sum (F_x{}^2 + F_y{}^2)}$ / N
5:	Initialize iteration counter: num ← 0
6:	while errorfunc > tol and num < maxit do
7:	Compute Jacobian matrix J for the residual equations
8:	Solve for updates: Δ ← $-J^{-1}F_{total}$
9:	Update X: X ← X + h · ΔX
10:	Update Y: Y ← Y + h · ΔY
11:	Recompute residuals F_x, F_y and update errorfunc
12:	update iteration count: num ← num + 1
13:	end while
14:	Record orbit information for the current ω
15:	end for

DOI: 10.54254/2753-8818/2025.DL27345

The main outputs X.txt and Y.txt are ($x(\theta_j)$, $y(\theta_j)$) coordinates along a period for each ω defined in input.txt. While the code also generates a PDF overview of orbits (as in Figures 3 and 4), users can perform detailed analysis of the X/Y.txt files using external Python scripts or other tools.